Automatic Modulation Recognition in the 868 MHz Wireless Network using Tree-Based Methods

by

Ken Lau

B.Sc., The University of British Columbia, 2013

A PROJECT SUBMITTED IN PARTIAL FULFILLMENT OF
THE REQUIREMENTS FOR THE DEGREE OF

MASTER OF SCIENCE

in

The Faculty of Graduate Studies

(Statistics)

THE UNIVERSITY OF BRITISH COLUMBIA

(Vancouver)

April 14, 2015

© Ken Lau 2015

Abstract

Wireless communication systems enable the transfer of data between devices through the transmission of radio signals. These wireless devices often transmit a variety of waveform types called modulation formats. Misidentification of modulation formats between two communicating devices could lead to undesirable delays in data transfer. The role of automatic modulation recognition (AMR) is the identification of the different modulations of transmitted signals. In this project, we apply AMR in the 868 MHz frequency band. A recent work implements a feature-based tree classifier for AMR. We extend the recent approach by implementing classification tree and random forest classifiers, as well as introduce an expanded list of features. Our classifiers are trained to identify six different modulations, as well as the detection of noise from signal.

Preface

This project is submitted in partial fulfillment of the requirements for a Master of Science in Statistics. It contains work from January 2014 to December 2014 under the supervision of Lutz Lampe and Matías Salibián-Berrera from the Electrical and Computer Engineering and Statistics Departments at UBC.

Table of Contents

List of Tables

List of Figures

Chapter 1

Introduction

Wireless communication has become very important in our daily lives as Wifi is pervasive at home, workplace, airports, and street corners. Wifi is aimed at long-distance communication, and involve applications that require a higher bandwidth and data transfer rate compared to most other wireless networks. This project is concerned with a Zigbee network which is similar to Wifi in the sense that Zigbee is also used for wireless communication. The difference is that Zigbee is targeted at short-distance communication and involves lower-powered and lower-data-rate applications. Examples of these applications are home temperature and light sensors, security devices, and wall-mounted switches. These applications do not require a high bandwidth, thus have lower costs to maintain. Devices using Zigbee operate on the 868 MHz frequency band.

We give a simple example of how two devices in a network interact. For simplicity, let us assume that data transfer is unidirectional, that is, signal is strictly sent from one device to another and not in the reverse direction. The bidirectional case is similar, but requires more work to explain. For example, Figure 1.1 shows a home temperature device transmitting a signal to a heater device. When the signal reaches the heater, data is extracted from the signal. For instance, the extracted data might contain information about the current temperature of the room, and so the heater adjusts the amount of electrical energy converted to heat accordingly. In case the reader is interested in wireless networks in general, chapter six of [1] provides detailed explanation of networks.

The home temperature and heater devices are examples of devices that use the 868 MHz frequency band. The signals transmitted from these devices generally transmit signals of six different waveforms, which are often referred to as modulation types in the IEEE literature. The receiving device, which is the heater in our example, should be able to identify these waveforms in order to process and extract data from the signal. The role of an automatic modulation recognition (AMR) method is the classification of modulations on the received signals. We implement classifiers that take a set of feature variables and a single class variable, and predicts the class variable on future

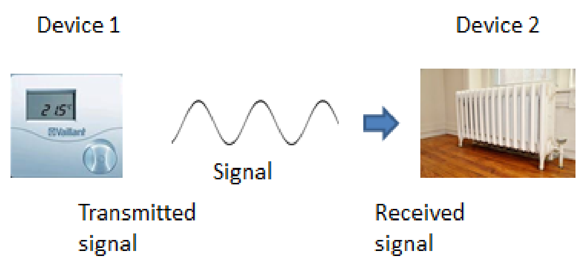

Figure 1.1: Example of signal transfer between two devices. Device 1 is a home temperature device which transmit signals to a heater device which is labeled as device 2.

data. Without a classifier, the receiver would only recognize the signals one sixth of the time, given there are six different waveforms.

We provide a simple example involving a classifier to predict tomorrow's weather given some atmospheric attributes of today's weather. The purpose of this example is to introduce the idea of machine learning and to ease us into AMR. The data is presented in Table 1.1. The first three columns correspond to the features and each of them describe atmospheric attributes of today's weather. The features are the amount of rain, humidity level, and percentage of sunshine for a particular day. The class variable is the weather condition for the next day given a particular day. A decision tree classifier can be constructed based on observing the pattern between the features and class variable. For example, based on the data, we might predict that there is rain tomorrow given the average amount of rain today was greater than 2mm. An example of a decision tree classifier might look like one given in Figure 1.2. Evidently, the tree appears to be constructed in a fairly ad hoc manner.

In the context of our study, the class variable corresponds to the modulation type. The set of feature variables is extracted from the transmitted signals. The modulation type and feature variables are further described in Sections 2.1 and 2.2 respectively. Figure 1.3 shows that the classifier receives the signal before being processed by the heater device. In fact, the classifier is integrated within the receiving device. Classifiers are described further in Section 3.1.

A feature-based tree classifier using strategically engineered features is implemented in [2]. This method is explained in 3.2. Similar to the classifier used in the weather prediction example, the features are chosen in a

Rain	Humidity	Sunshine	Weather Tomorrow
1mm	82%	9%	Cloudy
3mm	85%	40%	Rainy
0mm	80%	80%	Sunny
1mm	84%	5%	Cloudy
..	..	..	..

Table 1.1: Weather prediction example. The feature variables are amount of rain, humidity level, and percentage of sunshine today. The class prediction variable is the weather for tomorrow consisting of rainy, cloudy, or sunny.

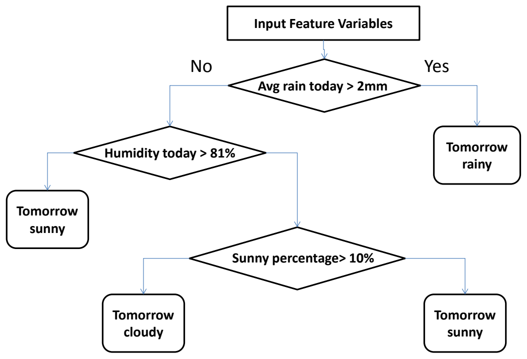

Figure 1.2: A classifier for the weather prediction data. Avg stands for average.

fairly ad hoc manner. Therefore, in this project, we extend the approach by implementing a classification tree that considers many more combinations of features and thresholds in constructing the tree. We further consider the random forest classifier that takes a consensus of predictions from numerous classification trees. The classification tree and random forest classifiers are described in Sections 3.3 and 3.4 respectively. We also implement an expanded list of features that improve the predictive performances of these classifiers described in Section 2.2.3. We obtained the idea from the papers in [3, 4], which provide an overview of common feature variables and classification algorithms applied to AMR tasks. The two papers also summarize the type of features that deem to improve different classifiers in AMR. For example, [4] provides suggestions as to which classifiers are useful for tree-based methods. In this project, we take it a step further, and implement most of the classifiers suggested in those papers in a addition to the entire spectrum (which is explained in Section 2.2.3). Finally, we train the classifiers to predict six different waveforms as well as identify signal from noise as described in Section 3.5.

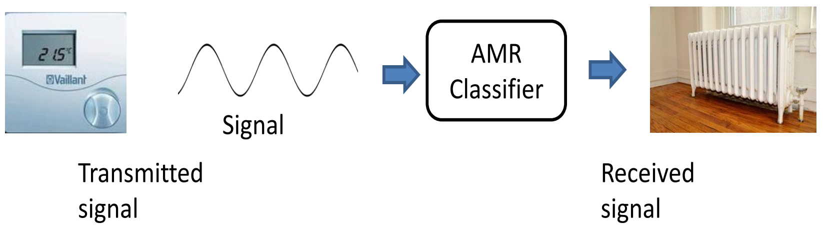

Figure 1.3: Example of signal transfer between two devices with classifier installed.

1.1 Other Related Work

Although this project involves only tree-based methods, we now describe other non tree-based methods that are often used in AMR tasks. An artificial neural network (ANN) is implemented in [5]. In fact, three ANNs are used in total to classify six types of digital modulation signals. For simplicity, let us identify these modulations using integers from 1 through 6. The objective function for all three ANNs is the proportion of correct classifications. The first ANN uses two hidden layers with 12 nodes in the first layer and 15 in the second. The first hidden layer of the first ANN uses a log-sigmoid loss function, while the second hidden layer uses a linear function. The method classifies modulations 1 and 2, but groups together modulations 3 and 4 as well as 5 and 6. The method is best understood in a visualization as provided in Figure 1.4. The second and third ANN do not use any hidden layers. A comparison between a feature-based tree approach and ANN is also shown in [5]. The results show that ANN provided an increase of 2% in predictive performance as opposed to the feature-based tree. However, a disadvantage of using ANN is the interpretation of the model. For example, it is difficult to determine how the prediction would change given we modify the values of some features. However, in the feature-based tree, we immediately know how the prediction would change given we increase or decrease certain values of features. Constructing an ANN is also a difficult task as there are many parameters to consider such as the number of hidden layers, nodes at each layer, and loss function of hidden layers. In addition, it should be apparent that the computation time of neural networks is usually far greater than a feature-based tree. In particular, the tree we built from the weather prediction example took little time to build. More details regarding the computational complexity of neural networks is provided in [6].

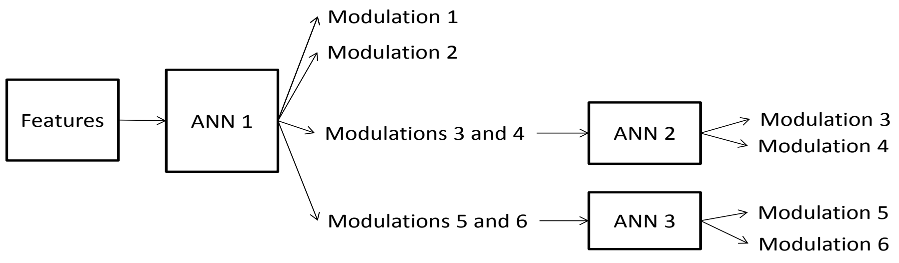

Figure 1.4: The visualization of using three ANNs to classify six modulations. Each ANN uses a single hidden layer.

Chapter 2

Data Simulation

We first describe the transmission of the signals for six different waveforms where simulations are performed in the Communications Toolbox of MATLAB [7]. Next, we show how the signals are preprocessed. Finally, we provide details about the features that are extracted from the signals.

2.1 Transmitting Signals

Recall that we are interested in the devices that use the 868 MHz frequency band which are found in the Zigbee network. These devices generally transmit six different modulation types. Three of the modulations include on-off keying (OOK), binary phase-shift keying (BPSK) and offset quaternary phase-shift keying (OQPSK). Each of these have a carrier frequency of 868.3 MHz which is just the frequency of the radio signal as it propagates from the transmitter to receiver device, for example in the introduction section, from the temperature to heater device. The other three modulations are the binary frequency-shift keying (BFSK) operating at carrier frequencies of 868.3 MHz, 868.95 MHz, and $868.03 + b \cdot 0.06$ MHz, where $0 \leq b \leq 9$, respectively. These are used in the wireless meter-bus specification which is a section of the device, and according to this specification, we denote the three modulation types as BFSK-A, BFSK-B, and BFSK-R2, respectively. Figure 2.1 provides a visualization of the differences between three general types of modulations, and where each of the six waveforms in our study resides on. The input signal data is a random sequence of zeros and ones. OOK belongs to amplitude shift keying (ASK) where the signal has zero amplitude when the input is zero. Evident from the figure, frequency shift keying (FSK) affects the frequency of the signal for different inputs, whereas phase shift keying (PSK) affects the phase of the signal for different inputs. Further details regarding the six communication signals are provided in [2].

At the receiver, the signals are mixed to a low intermediate frequency. One reason in using an intermediate frequency is to improve the performance in which a radio receiver respond to a signal. In other words, it is useful in

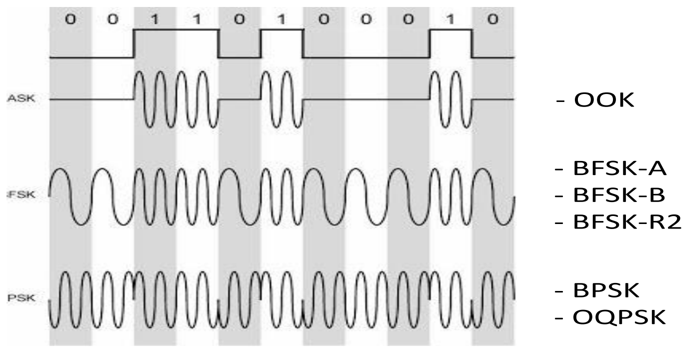

Figure 2.1: Behaviors of the modulations. OOK belongs to amplitude shift keying (ASK), BFSK-A, BFSK-B, and BFKS-R2 belong to frequency shift keying (FSK), and BPSK and OQPSK belong to phase shift keying.

the encoding and decoding of the radio signals in the stages of amplifiers, filters, and detectors. It does not directly affect the automatic modulation recognition (AMR) task we are studying, but we should be consistent with how the rest of the device is integrated, and use the same intermediate frequency throughout. Therefore, for our numerical results presented in Section 4, we apply down-conversion by 867.3 MHz, i.e., the intermediate frequency for OOK modulation would be 1 MHz. Down-conversion means subtracting the frequency by 867.3 MHz. The signal at intermediate frequency is sampled with sampling frequency f_s, resulting in the discrete-time signal $r[k]$, where k is the discrete-time index. As in [2], we apply a sampling frequency $f_s = 6.25$ MHz. The received signal is expressed as

$$r[k] = s[k] + n[k] \ , \tag{2.1}$$

where $s[k]$ is the subtracted and sampled transmitted signal and $n[k]$ is white Gaussian noise with variance σ_n^2. Denoting the variance of $s[k]$ by σ_s^2, we define the signal to noise ratio (SNR) as σ_s^2/σ_n^2.

The task of AMR is to determine from the received signal $r[k]$ which of the six modulation formats has been used in $s[k]$. To this end, features are extracted from $r[k]$ and then used in a classifier. The features and classifiers applied in previous and our AMR approaches will be introduced next.

2.2 Feature Extraction

This section describes the preprocessing of the received signals, followed by how features are computed.

2.2.1 Preprocessing

The task of AMR begins by preprocessing N samples of the sampled received signal in 2.1. Following [2], we adopt $N = 512$ and generate via discrete Fourier transform (DFT) the spectral representations

$$R[k] = \sum_{i=0}^{N-1} r[i]e^{-j2\pi\frac{ik}{N}} \ , \quad k = 0, \dots, N-1 \tag{2.2}$$

and

$$A[k] = \sum_{i=0}^{N-1} \frac{|a[i]|}{\mu_a} e^{-j2\pi\frac{ik}{N}} \ , \quad k = 0, \dots, N-1 \ , \tag{2.3}$$

where ($\mathcal{H}\{\cdot\}$ denotes Hilbert transformation and j is an imaginary number.)

$$a[i] = r[i] + j\mathcal{H}\{r[i]\} \ , \quad i = 0, \dots, N-1 \tag{2.4}$$

is the analytic received signal and

$$\mu_a = \frac{1}{N}\sum_{i=0}^{N-1} |a[i]| \ . \tag{2.5}$$

According to the Matlab documentation [8], the Hilbert transformation returns the original sequence with a $90\,^\circ$ phase shift. This simply means, for example, that sines are transformed into cosines. The equation, $A[k]$, is the DFT of the normalized absolute analytic signal. The analytic signal is required in computing some of the features such as the transformation based features in Section 2.2.3.

2.2.2 Features From [2]

Let the features required in the feature-based binary tree in [2] be denoted as m_1, m_2, m_3, m_4, and m_5. Feature m_1 is computed as follows,

$$m_1 = max(|A[k1]|) + max(|A[k2]|) \tag{2.6}$$

where $1 \leq k_1 \leq 7$ and $25 \leq k_2 \leq 27$. Next, we compute m_2 and m_3:

$$m_2 = \frac{A[k_2]}{max(A[k_1])} \tag{2.7}$$

$$m_3 = \frac{|R[k_4]|}{R[k_3]} \tag{2.8}$$

where k_3 is defined as the index of the maximum value of $|R[k]|$ and k_4 is the second largest value with at least four indices away from k_3. Finally,

$$m_4 = \left\lfloor \frac{k_3 + k_4 + 1}{2} \right\rfloor, \tag{2.9}$$

and

$$m_5 = \frac{\sum_{k=m_4-B_2/2}^{m_4+B_2/2} |R[k]|}{\sum_{k=m_4-B_1/2}^{m_4+B_1/2} |R[k]|} \tag{2.10}$$

where $B_1 = 36$ and $B_2 = 18$.

2.2.3 Additional Features

In this section, we implement additional features for the AMR. The type of features we describe are commonly used in AMR problems, e.g. cf. [4, 9–11].

Transformation Based Features

The first set of proposed features is related to the spectral representation of the analytical signal. More specifically, we compute the maximal squared magnitude frequency component

$$\gamma_{\max} = \max_{k=0,\ldots,N-1} \frac{1}{N} |A[k]|^2. \tag{2.11}$$

Since $\gamma_{\max}$ corresponds to amplitude variation of signals [4], this feature is useful in discriminating between OOK and the PSK/FSK modulations, because OOK is the only amplitude shift keying modulation. Therefore, the only modulation we expect amplitude variation is of course, OOK. Furthermore, the maximum value of the DFT of the 2^{nd} and 4^{th} power of the analytical form is computed, i.e.,

$$\Gamma_n = \max_{k=0,\ldots,N-1} \frac{1}{N} \sum_{i=0}^{N-1} |a[i]|^n e^{-j2\pi \frac{ik}{N}} , \tag{2.12}$$

for $n = 2$ and $n = 4$. The features, Γ_2 and Γ_4 are useful in classification of PSK signals. In particular, these features discriminate BPSK and OQPSK modulations from the remaining modulations. Similar to the amplitude variation case, we expect that the only modulations to obtain phase variation are BPSK and OQPSK.

Higher-Order Cumulant Features

Each modulation has a different in-phase and quadrature (I-Q) component which is often represented by a constellation diagram. For example, Figure 2.2 depicts constellation diagrams for BPSK and OQPSK. The x and y axes represent the in-phase and quadrature components of the modulation respectively. For instance, the two circles labeled with 0 and 1 for BPSK represent the symbols, and indicate the two phases with a shift separation of 180 °. The four circles of the constellation diagram for OQPSK represent its four symbols and the 90 ° shift separation. In fact, the I-Q components are

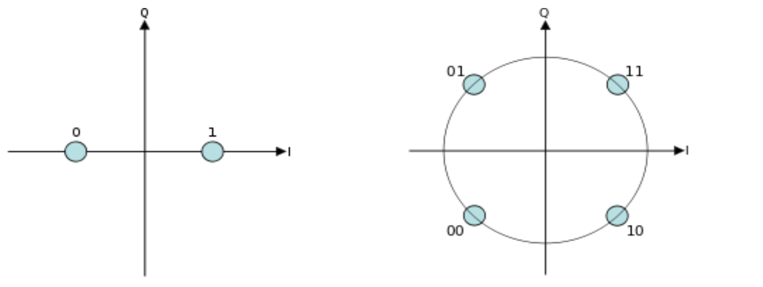

(a) Binary Phase Shift Keying (BPSK) (b) Offset Quadrature Phase Shift Keying (OQPSK)

Figure 2.2: Constellation diagrams for BPSK and OQPSK.

related to the real and imaginary components of the signal [9]. The in-phase component is shown on the x-axis which also resembles the real component of the modulation. Similarly, the quadrature component is shown on the y-axis which also resembles the complex component of the modulation. This leads us to why we are computing the higher-order cumulant (HOC) features. The HOC features are based on the non-linear combinations of the real and imaginary components of the analytical signal as shown in Equation 2.13 below. By computing the higher-order cumulant (HOC) features, we can capture the real and imaginary parts of the signal, which in turn discriminates different modulations based on the I-Q components and constellation diagrams.

At this point, we calculate the real and imaginary parts of the analytical signal from Equation 2.4, and denote either parts as $x_i[0], x_i[1], \ldots, x_i[N-1]$. A signal vector is represented as $X_i = \{x_i[0], x_i[1], \ldots, x_i[N-1]\}$ for some i. For all combinations of $X_i, i = 1, \ldots, 4$ based on the real or imaginary parts of the analytical signal, we compute the following equations:

$$\begin{aligned} C_{X_1X_2} &= \frac{1}{N}\sum_{k=0}^{N-1} x_1[k]x_2[k] \\ C_{X_1X_2X_3} &= \frac{1}{N}\sum_{k=0}^{N-1} x_1[k]x_2[k]x_3[k] \\ C_{X_1X_2X_3X_4} &= \frac{1}{N}\sum_{k=0}^{N-1} x_1[k]x_2[k]x_3[k]x_4[k] - C_{X_1X_2}C_{X_3X_4} \\ &\quad - C_{X_1X_3}C_{X_2X_4} - C_{X_1X_4}C_{X_2X_3} \end{aligned} \tag{2.13}$$

$X_i, i = 1, \ldots, 4$ can be either the real or imaginary signal vector of the analytical signal. As an example, we can compute the real part of the analytical signal and denote it as a signal vector X_1, and imaginary part as X_2. Using X_1 and X_2 we compute $C_{X_1X_2}$. The cumulants are also called the time-averaging approximations of the second, third, and fourth order cumulants.

Magnitude Spectrum

The last set of proposed features consists of the magnitude spectrum, $|R[k]|$ for frequency indexes of $k = 45$ to $k = 160$. These features are particularly useful in detecting the BFSK-B modulation, as it is modulated at a higher carrier frequency than the remaining modulations. Figure 2.3 depicts the magnitude spectrum for each of the modulations at a SNR of 11 dB. At the best of our knowledge, the collection of these features has not been used in any AMR tasks, therefore we did not expect a major impact in terms of performance on the classifiers. However, our analysis in Section 4.2 begs differently. It turns out that many of the magnitude spectrum features contributed towards the random forest classifier based on Figure 4.6. We summarized all the features in the Table 2.1.

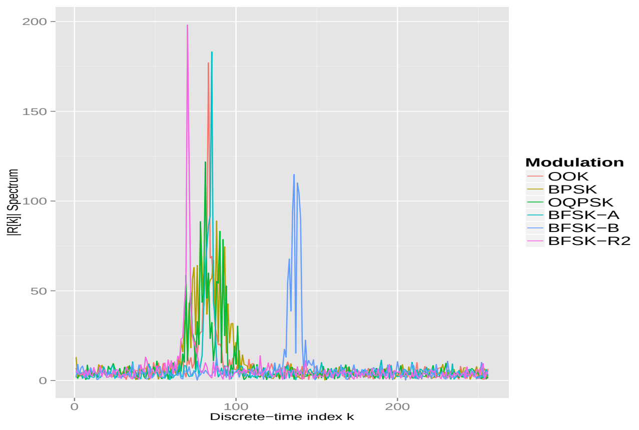

Figure 2.3: Magnitude spectrum, $|R[k]|$ at SNR of 11 dB. The x-axis corresponds to the discrete-time index.

Table 2.1: Summary of feature variables.

Description	**Features**
Features from [2]	$m_1, m_2, \ldots, m_5$
Transformation-based	$\gamma_{\max}, \Gamma_2, \Gamma_4$
Higher-order cumulant	$C_{II}, C_{IQ}, C_{QQ}, C_{III}, C_{IIQ}, C_{IQQ}, C_{QQQ}, C_{IIII}, C_{IIIQ}, C_{IIQQ}, C_{IQQQ}, C_{QQQQ}$
Magnitude spectrum	$\{\lvert R[k]\rvert \mid k = 45, \ldots, 160\}$

Chapter 3

Implementation

We now turn to the use of the features in the classification methods. We first briefly discuss the choice of a training data set and review the implementation of the feature-based tree (FBT) from [2]. Then we present the proposed classification tree (CT) and random forest (RF) classifiers. Finally, we describe the modifications required in order to detect true white noise signals.

3.1 Training Data

In the introduction, we mentioned that the class variable is the modulation type, while the feature variables are just the ones summarized in Table 2.1. Let us recall the data set from the simple weather prediction example shown in Table 1.1. This data set represents the training data, as the decision tree classifier was constructed on the basis of this data set. The training data set is generated from a Monte-Carlo simulation, obtaining P values for each feature variable per modulation and SNR value. We provided a visualization example of the process of generating a single observation in Figure 3.1. The signal is first transmitted from the device, and then noise is added to the signal to get our received signal, $r[k]$. At this point, $r[k]$ is preprocessed, and features are extracted from the signal. So, in the example, the received signal is first obtained by transmitting a signal using an OOK modulation, and then noise is added to the signal in order to obtain a SNR of 10 dB. Using the received signal and some pre-processing steps as described in Section 2.2.1, all the features are computed. This represents a single observation. This same process is performed P times for every modulation and SNR. Section 4 describes the specification of P and range of SNR considered. We provided an example of the data in Table 3.1. The modulation column corresponds to the class variable, while the columns to the right of the modulation column correspond to the feature variables.

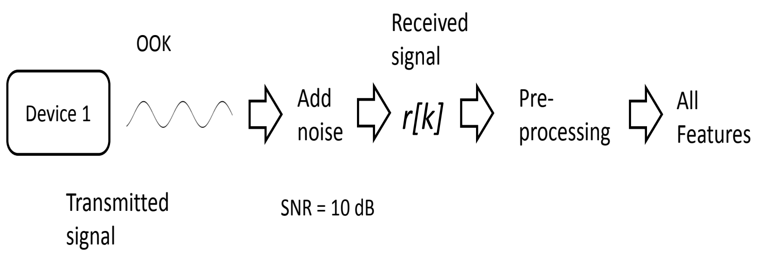

Figure 3.1: Process of generating one observation of the training data.

Table 3.1: Example of training data. The modulation corresponds to the class variable, and the columns to the right of modulation from m_1 to R[160] correspond to the feature variables.

Modulation	$\boldsymbol{m_1}$	$\boldsymbol{m_2}$	$\boldsymbol{m_3}$	**...**	**R[160]**
OOK	190	0.05	0.3	...	2.5
OOK	186	0.12	0.21	...	1.8
OOK	172	0.08	0.25	...	3.1
..	..	..	..	..	..
BFSK-R2	15.3	0.64	0.03	...	5.4
BFSK-R2	14.4	0.54	0.08	...	3.3
BFSK-R2	89.7	0.35	0.12	...	2.48

3.2 Feature-Based Binary Tree

The feature-based binary tree (FBT) classifier utilizes features from [2], and selects thresholds that discern different modulation types. The construction of the FBT is very similar to the decision tree classifier for the weather prediction example described in the introduction section. The first split of the tree is chosen based on the feature m_1. Next, a threshold value of m_1 must be determined. Figure 3.3 shows the distribution of values of m_1 using a boxplot, where the red lines indicate the minimum and maximum values of BPSK and BFSK-A, and the purple line shows the gap between the min and max of BPSK and BFSK-A respectively. It is easy to see that m_1 values above a certain threshold discern OOK and BPSK from the remaining modulations. Therefore, it makes sense to choose a value that is within the gap formed by the minimum m_1 value of OOK or BPSK and the maximum m_1 value of OQPSK, BFSK-A, BFSK-B, and BFSK-R2 as shown by the

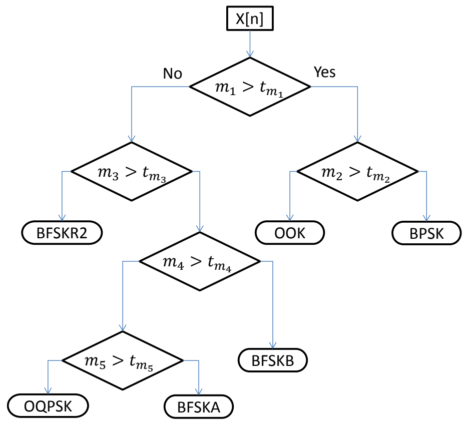

Figure 3.2: Flowchart of feature-based tree depicting features and decision thresholds at interior nodes. Modulation types reside at leaf nodes.

purple line. In [2], not all the modulations were used to determine this gap, and only BPSK and BFSK-A were chosen for m_1.

In order to determine the threshold, a worst-case analysis between m_1 values of BPSK and BFSK-A is performed. Figure 3.4 presents the maximum and minimum value of m_1 for BPSK and BFSK-A respectively. Similar to the boxplot visualization, the gap between the min value of m_1 of BPSK is compared with the max value for BFSK-A using a purple line. As we can see from the figure, as SNR increases, the gap shrinks. The threshold is chosen as the value of m_1 where the gap reaches zero. In [2], not all the modulations were used to determine this gap, and only BPSK and BFSK-A were chosen for m_1. Figure 3.4 depicts the worst-case analysis between m_1 values of BPSK and BFSK-A. The gap reaches zero when the two lines in the plot intersects. The intersection appears approximately at 4.7 dB with a threshold of $t_{m_1} = 47$. Consequently, signals with $m_1 > 47$ are classified as either OOK or BPSK, while signals with $m_1 \leq 47$ are classified as one of the remaining modulations. The thresholds for $m_2, \ldots, m_5$ are determined similarly, see [2] and Table 3.2. Additional details for the threshold determination can be found in [2]. The tree is presented in Figure 3.2. Finally, a prediction is made by traversing down the tree until a leaf node is reached.

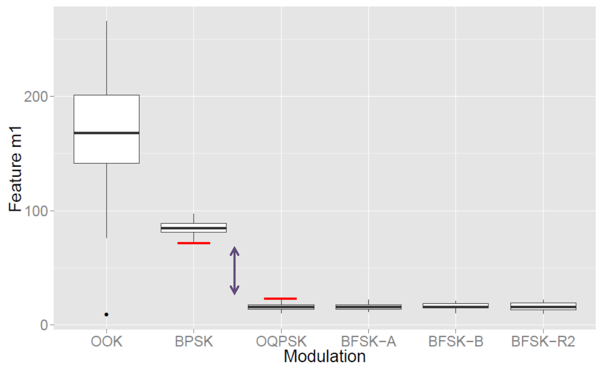

Figure 3.3: Boxplot visualization of m_1 for each modulation.

	Feature	**Threshold**
1	m_1	47.23
2	m_2	0.42
3	m_3	0.23
4	m_4	89.68
5	m_5	0.71

Table 3.2: Thresholds determined by FBT.

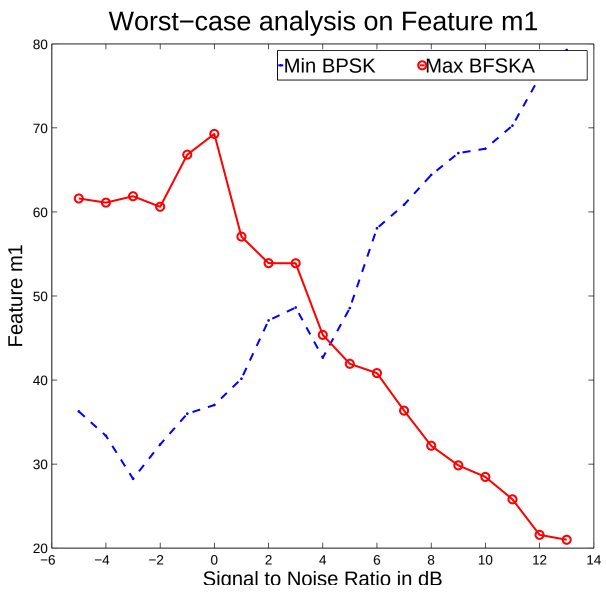

Figure 3.4: Worst-case analysis plot of m_1. Solid line corresponds to the maximumim of m_1 of BFSK-A. Dashed line corresponds to the minimum of m_1 of BPSK.

3.3 Classification Tree

The first classifier we propose is a classification tree (CT). Similar to the FBT, it also selects thresholds using a set of features. However, the thresholds are chosen differently. First, let us denote the class variable as a discrete random variable called Y. This variable takes on six values corresponding to the six different modulations. For simplicity, let us use integers from one to six as values of Y in place of the modulation names in the respective order as OOK, BPSK, OQPSK, BFSK-A, BFSK-B, and BFSK-R2. Let us also define continuous random variables X_u for $u = 1, 2, \ldots, M$ for the M feature variables considered as in Table 3.1. Furthermore, let us denote the training data set as $\mathscr{D} := \{(y_i, \mathbf{x_i})\}_{i=1}^{n}$ where y_i and $\mathbf{x_i} = (x_1, x_2, \ldots, x_M)^T$ refer to the observed values of Y and the feature variables respectively.

We use T to denote the total number of observations of $\mathscr{D}$, and n_l as the number of observations of modulation l where $l = 1, 2, \ldots, 6$. The probability mass function (PMF) for Y is defined as

$$P(Y = l) = p_l = \frac{n_l}{T}.$$

To determine the thresholds of the classification tree, we must determine which feature to split by and what value of threshold to use for the feature. So, let us further define the conditional discrete random variables $Y|X_u < t_u$ and $Y|X_u \geq t_u$ for some $u = 1, 2, \ldots, M$ and threshold value t_u. The PMF of $Y|X_u < t_u$ is similar to Y, except we consider only $\mathscr{D}$ for which the feature variable u have values less than t_u. Another way to look at this is that u represents a feature chosen as the split and t_u represents the threshold of this split. We use T_{lower} to represent the number of observations for this new partition of the data set $\mathscr{D}_{lower}$. The proportion of observations corresponding to this region is

$$p_{lower} = \frac{T_{lower}}{T}.$$

Also, let $n_{lower,l}$ represent the number of observations corresponding to modulation l in this lower region. The PMF for $Y|X_u < t_u$ is then,

$$P(Y|X_u < t_u) = p_{lower,l} = \frac{n_{lower,l}}{T_{lower}}$$

The PMF for $Y|X_u \geq t_u$ is similarly defined except we use $\mathscr{D}_{upper}$ for which $X_u \geq t_u$ and

$$p_{upper} = \frac{T_{upper}}{T}.$$

To determine the first split of the tree, we need to choose a feature u and threshold t_u which minimizes the entropy loss function on the resulting split. We should mention that other loss functions are commonly used as well for CT such as misclassification error and gini index, but we are going to focus on entropy. The entropy, $\mathbb{H}$ of Y is defined as follows,

$$\mathbb{H}(Y) = -\sum_{l} p_l log(p_l). \tag{3.1}$$

Similarly, the entropy of $Y|X_u < t_u$ is computed as follows,

$$\mathbb{H}(Y|X_u < t_u) = -\sum_{l} p_{lower,l} log(p_{lower,l}) \tag{3.2}$$

The entropy $\mathbb{H}(Y|X_u \geq t_u)$ is similarly computed. Finally, the feature u and threshold t_u chosen is the threshold minimizing the following quantity:

$$p_{lower} \cdot \mathbb{H}(Y|X_u < t_u) + p_{upper} \cdot \mathbb{H}(Y|X_u \geq t_u).$$

Let us denote the minimal entropy found in the above equation by ent, in other words we have:

$$ent = \min_{u,t_u}\{p_{lower} \cdot \mathbb{H}(Y|X_u < t_u) + p_{upper} \cdot \mathbb{H}(Y|X_u \geq t_u)\} \tag{3.3}$$

If $ent < H(Y)$, then we recursively apply the same process of determining an optimal threshold on both $\mathscr{D}_{lower}$ and $\mathscr{D}_{upper}$ until $ent \geq H(Y)$. When a partition of the data where $ent \geq H(Y)$ for all possible splits, a prediction is made based on the value with the highest probability as defined by the PMF on the that particular region of the training data. This recursive procedure is best understood by a visualization as shown in the following paragraph. Additional details on CTs can be found in [12].

We present a simple example to illustrate the algorithm used to construct a CT as shown in the sequence of Figures 3.5 to 3.9. Figure 3.5 depicts the example data set. There are two feature variables denoted as x1 and x2, and one class variable with two possible values: red or blue. There are 53 observations in total, where 26 of them are labeled as blue and 27 of them red. The data set, $\mathscr{D} = \{(y_i, \mathbf{x_i})\}_{i=1}^{53}$ contains all the points in the figure. The random variable Y for the class variable takes on two values: blue and red. Based on $\mathscr{D}$, the PMF of Y has $p_{blue} = \frac{26}{53}$ and $p_{red} = \frac{27}{53}$ for blue and red points respectively. The entropy is computed using Equation 3.2 to be 0.69.

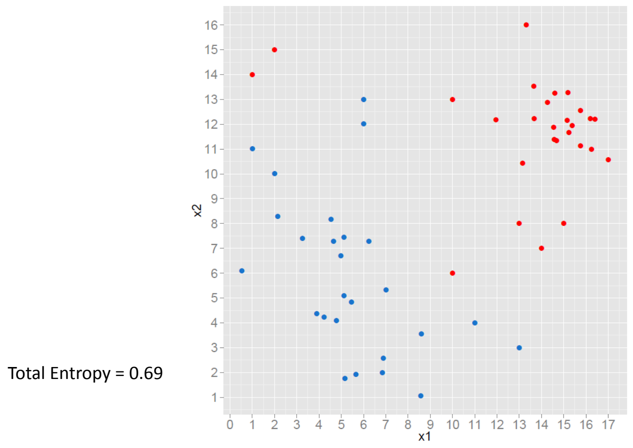

Figure 3.5: Example of data with two feature variables denoted as x1 and x2. The class variable takes on two values of either blue or red. There are 53 observations in total, where 26 are labeled as blue and 27 as red.

Next, we want to determine whether to split on feature x_1 or x_2. It seems like the optimal split is x_1 since there does not appear to be a good split using x_2 that would partition the data with high proportions of each color in each region. Let us choose the value $x_1 = 10.5$ as the first split as shown in Figure 3.6. The two regions are encapsulated by the two purple rectangle, and the entropy of the left and right regions are computed to be 0.41 and 0.28 respectively. We obtained $ent = 0.35$ which is lower than 0.69 so we could split by this threshold value of $x_1 = 10.5$. However, this split is not optimal as we explain in the next paragraph.

The optimal split actually occurs at x_1 anywhere from 8.7 to 10, since this split results in both regions with highest proportion of each color (blue on the left region and red on the right). We will use $x_1 = 9.5$. Noting that X_1 and X_2 are the random variables of the feature variables, the PMF of $Y|X_1 < 9.5$ and $Y|X_1 >= 9.5$ can be computed. Let us refer to the left and right region data as $\mathscr{D}_{lower}$ and $\mathscr{D}_{upper}$ as described previously. The PMF of $Y|X_1 < 9.5$ is $p_{lower,blue} = \frac{26}{28}$ and $p_{lower,red} = \frac{2}{28}$. Using the entropy function of Equation 3.2, we computed $\mathbb{H}(Y|X_1 < 9.5) = 0.271$. Similarly we computed the entropy of the right side $\mathbb{H}(Y|X_1 >= 9.5) = 0.264$. We computed ent for this split to be $ent = 0.27$, so we designate our first split as

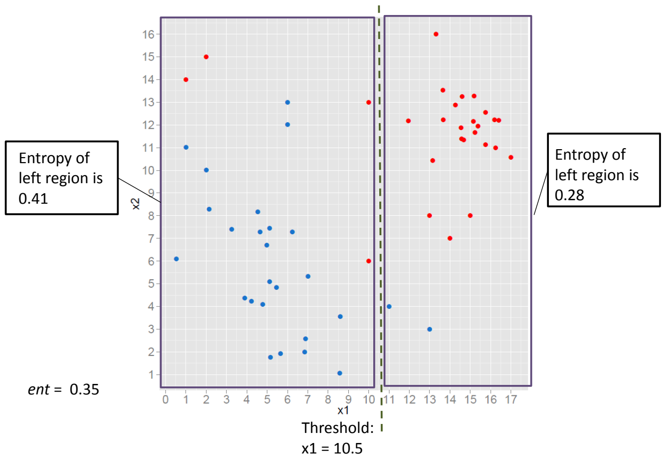

Figure 3.6: A sub-optimal split would be choosing variable x1 = 10.5. Then entropy of the left and right region indicated by the purple rectangle windows are computed to be 0.41 and 0.28 respectively.

$x_1 = 9.5$, and we continue splitting on the left and right regions recursively.

Next, consider the left region of the split as shown by Figure 3.8. For the sake of brevity, let us re-use notations to denote the current left region of data as $\mathscr{D} \leftarrow \mathscr{D}_{lower}$ and treat this region as the current training data. Likewise we define random variables Y, X_1, and X_2 for this new data set $\mathscr{D}$ with the same functions as before.

It is clear that a value of x_2 between 13 and 14 would be optimal since the two regions would only contain either blue or red points. The entropy of the region was computed previously to be 0.271. However, we need to determine the PMF of $Y|X_2 < 13.5$ and $Y|X_2 \geq 13.5$. The PMF of the former has $p_{lower,blue} = 1$ and $p_{lower,red} = 0$. Therefore, the entropy is computed to be 0 for the lower region. Likewise, the entropy for the upper region is computed to be 0. Thus, $ent = 0$ for this particular split and it is less than the entropy of the left region, so we designate the split as $x_2 = 13.5$ as the left child split of $x_1 = 9.5$. Since the proportions of blue/red points are either 0 or 1, there are no other splits which could reduce the entropy. Therefore, the algorithm stops there.

The same process occurs on the right side as shown in Figure 3.9. We found the split $x_2 = 5$ as the split and designate it as the right child split of $x_1 = 9.5$. Similarly no other split could reduce the entropy on the right

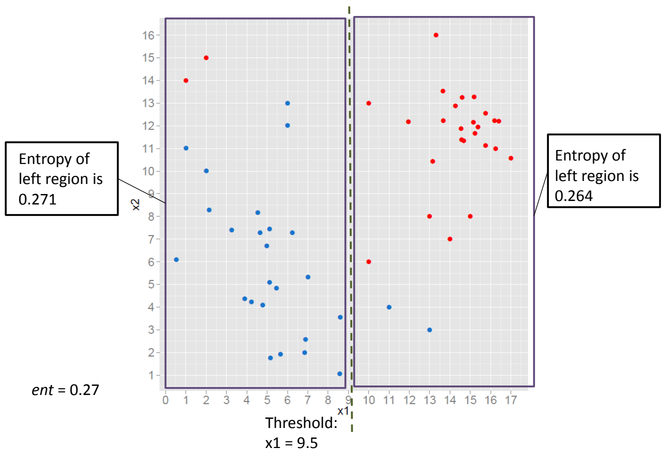

Figure 3.7: The optimal split is depicted by the dashed dark green line obtained by choosing variable x1 = 9.5. The entropy of the left and right region indicated by the purple rectangle windows are computed to be 0.271 and 0.264 respectively.

region, so the algorithm stops there. Ultimately, the tree of this simple example is displayed in Figure 3.10.

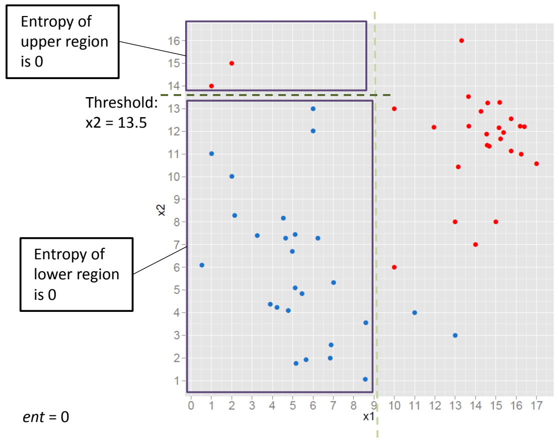

Figure 3.8: The optimal split is depicted by the dashed dark green line obtained by choosing the variable x2 = 13.5. The entropy of the bottom and upper region indicated by the purple rectangle windows are computed to 0 for both regions.

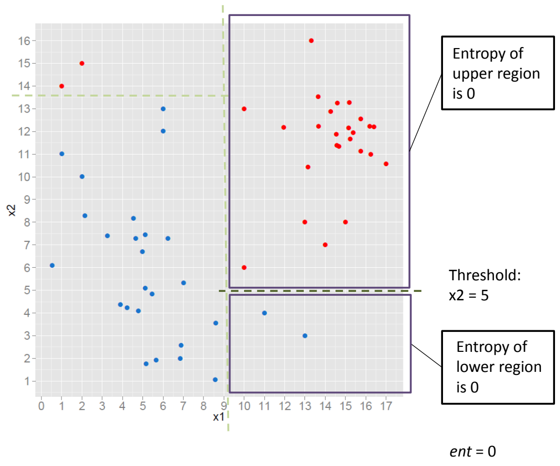

Figure 3.9: The optimal split is depicted by the dashed dark green line obtained by choosing the variable x2 = 5. The entropy of the bottom and upper region indicated by the purple rectangle windows are computed to 0 for both regions.

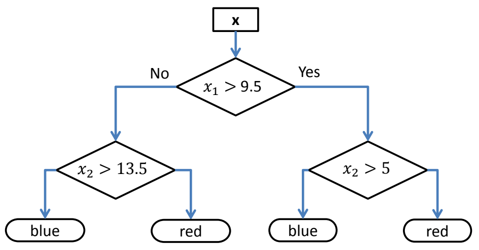

Figure 3.10: The tree structure of the simple classification tree algorithm shown in the sequence of figures 3.5 to 3.9.

Unlike the FBT, the CT classifier algorithm performs a more extensive search of the features and thresholds in constructing the tree. In particular, the CT allows the features to be selected any number of times, and it considered all variables and thresholds at each split. It also used a loss function, for which contributed towards constructing the tree. Classifications are made by traversing down the tree until a leaf node is reached. A new observation x_i (using the same notation when we defined $\mathscr{D}$) is classified to one of the six possible modulations using the tree we constructed in Figure 3.11 for the simple CT example we described.

3.3.1 Pruning

The complete tree is typically quite large, so pruning is performed by selecting the subtree with minimal splits while still minimizing the entropy of each split. The CT without pruning often overfits, because the algorithm that constructs the tree is so adaptive towards the data that adding or removing a few points could affect the tree mildly. For example, removing the two red points at the top left of Figure 3.5 would preclude the split shown in Figure 3.8. Another way to see it is that the complete tree is typically unstable, but pruning could remove some of this instability.

The implementation involves computing subsets of the tree and taking the subset of tree with the lowest misclassification error through a 10-fold cross-validation. We are not going to go over cross-validation as the method is very simple and there are many resources out there for that such as in [13]. For instance, the pruned version of the simple classification tree example might look like the tree of Figure 3.11. For more information about pruning classification trees, we refer the readers to [12].

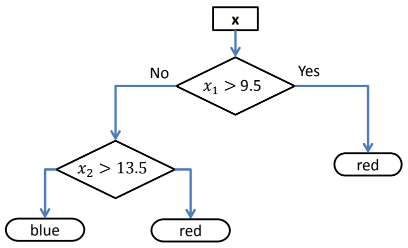

Figure 3.11: Pruned example of the simple classification tree example.

We apply the CT using features from Section 2.2.2 without and with

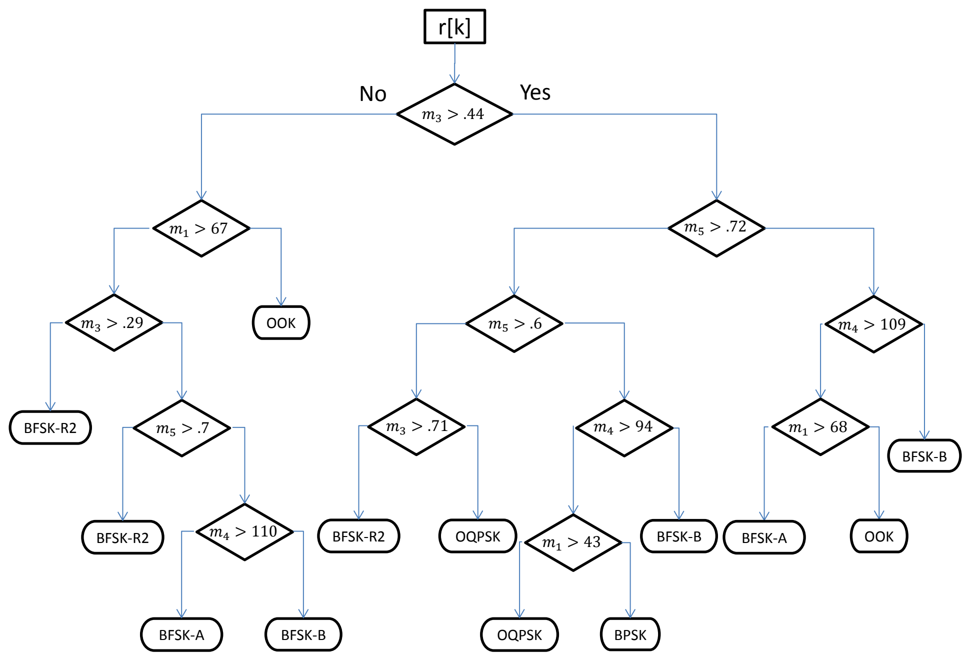

Figure 3.12: Flowchart of classification tree depicting features and decision thresholds at interior nodes. Modulation types reside at leaf nodes.

the additional features introduced in Section 2.2.3. Figure 3.12 illustrates an example of a CT based on the features from [2]. Evidently, the CT is considerably larger than the FBT, and features can appear more than once for the CT. Training was carried out through the rpart package in R [14].

3.4 Random Forest

Random forest (RF) utilizes a method known as bagging to average over numerous classification trees obtained by bootstrapping the original data [12]. By doing so, the RF leverages from the predictions acquired from all CTs so that the consensus achieves a more accurate prediction. We describe the implementation in the next paragraph. In addition, we show that the RF indeed improved the success rate over the CT in Figures 4.1 and 4.4 in Section 4.

The CTs are trained on bootstraps of the original training data set ($\mathscr{D}$) where the bootstrap sample is the same size as the $\mathscr{D}$. The implementation of RF begins by first drawing a bootstrap sample from $\mathscr{D}$. Let us call the bootstrap sample as $\mathscr{D}*$. At this point, a CT is trained using $\mathscr{D}*$ with a slight modification to the original CT algorithm in Section 3.3. The difference is that at each split, $m < M$ features are selected at random where M is the total number of features as describe previously. In addition, no pruning is performed on the trees. We repeat the process n_{tree} times where n_{tree} is a parameter, and we shall explain this later in this section. At the end, we have n_{tree} number of CTs which together forms a RF.

Classification of a new observation x_i is performed similarly to the CT, except we have n_{tree} CTs. Therefore, we have n_{tree} classifications. Let us refer to the b^{th} classification made by the b^{th} tree to be $\hat{C}_b(x)$. The classification of the RF is then $\hat{C}_{rf}(\mathbf{x}) = mode\{\hat{C}_b(\mathbf{x})\}_1^{n_{tree}}$ which is the majority vote prediction of the n_{tree} trees.

We have mentioned earlier that bagging involves the average over the CTs, but the prediction estimator ($\hat{C}_{rf}$) above is based on the mode of the prediction estimators of the CTs ($\hat{C}_b$) instead of the average. Since the predictions are discrete, we sought classification rather than regression. Intuitively, the idea of utilizing a collection of trees to improve the predictive accuracies are similar in both the regression and classification case. The analysis underlying the majority vote and the discrete prediction case is much more difficult, so we are going to analyze the continuous case instead.

Using the same notation for classification, the estimator of the classification is $\hat{C}_b(\mathbf{X})$ for a single tree which is also a random variable with no explicit form but instead implicitly defined by the tree constructed in the training stage (for example Figure 3.11). There are two ways to improve the predictive accuracy of a classifier. One way is to reduce the bias of the classification estimator for example on $\hat{C}_b(\mathbf{X})$. The bias of $\hat{C}_b(\mathbf{X})$ is

$$B(\hat{C}_b(\mathbf{X})) = \mathbb{E}(\hat{C}_b(\mathbf{X})) - Y \tag{3.4}$$

Under the regression case we have for the RF, $\hat{C}_{rf}(\mathbf{X}) = \frac{1}{n_{tree}} \sum_{i=1}^{n_{tree}} (\hat{C}_b(X))$. Furthermore, each $\hat{C}_b(X)$ is identically distributed because we bootstrapped from the original data and the same algorithm is executed on each of these data sets. Therefore, even if we do not have an explicit value of $\mathbb{E}(\hat{C}_b)$, the fact that $\hat{C}_{rf}(\mathbf{X})$ is an average of identically distributed random variables, the expectation of each of these estimators must be the same, and therefore the expectation of one of these estimators is the same as the expectation over the average of a collection of these estimators. Therefore, the bias of the prediction estimator of RF and CT are the same. The difference in the two estimators occur in analyzing the variance of these two estimators. We next show that the variance of the prediction estimator of RF is less than CT.

Firstly it should be clear that the prediction estimators of a collection of CTs are not independent, because we are using the same algorithm for each fit with the only difference occurring in the bootstrap samples. In fact, the pairwise correlations of these CTs are positive. Let us refer the variance of the prediction estimators to be σ^2, in other words, $Var(\hat{C}_b(\mathbf{X})) = \sigma^2$. Clearly, if the trees are independent, then $Var(\hat{C}_{rf}(\mathbf{X})) = \frac{1}{n_{tree}}\sigma^2$. However, the trees are likely positively correlated. Let us use ρ to refer to the pairwise correlation between two prediction estimators of two trees. In other words, $Cor(\hat{C}_i(\mathbf{X}), \hat{C}_j(\mathbf{X})) = \rho$ for some $i = 1, 2, \ldots, n_{tree}$ and $j \neq i$. The variance of the prediction estimator of RF is computed as follows:

$$\begin{aligned} Var(\hat{C}_{rf}(\mathbf{X})) &= \frac{1}{n_{tree}^2}(n_{tree}\sigma^2 + n(n-1)\sigma^2\rho) \\ &= \frac{\sigma^2}{n_{tree}} + \frac{(n_{tree}-1)}{n_{tree}}\sigma^2\rho \\ &= \sigma^2\rho + \frac{\sigma^2}{n_{tree}} - \frac{\sigma^2\rho}{n_{tree}} \\ &= \sigma^2\rho + \frac{1-\rho}{n_{tree}}\sigma^2 \end{aligned} \tag{3.5}$$

As n_{tree} increases the second term becomes small, so the variance is at least as large as $\sigma^2\rho$. This is an improvement since $-1 \leq \rho \leq 1$. Moreover, the less correlated the trees are the lower the variance, so at the end we are limited by the correlation of the trees which ultimately limit the advantages of bagging. This issue brings us back to why the RF algorithm involves randomly selecting $m < M$ features at each split rather than all M features at each split. Intuitively, selecting only subsets of the features allow the trees to be different which leads the trees to be less correlated. If we use all features at each split, then the trees would be very similar, hence, the prediction estimators would be very correlated.

Based on [12], fully growing the trees seldom cost much, and as a result, we have one less parameter to optimize. Therefore, we allow the trees to be grown to maximal depth. Model fitting was carried out using the randomForest package in R [15].

The parameters that require tuning in RF are the number of trees, $ntree$, and the number of randomly selected features, $mtry$. The number of trees should be large enough so that predictions are made multiple times for each observation [16]. Recall that each bootstrap sample retains roughly 63% of the original data, since the procedure involves randomly sampling from the same data set with replacement. In the worst-case scenario of not having enough trees is that not all the data have been used, which is bad since we always want to consider using all the training data.

A suitable value is around 500-1000 according to [12]. A large value of *ntree* often does not overfit or hinder the predictive performance of the model. However, as we have mentioned, *ntree* needs to be large enough so that predictions are made multiple times for each observation. In our experiments, we used $ntree = 850$ trees. The inventors of RF suggest $mtry$ to be approximately equal to the square-root of the number of features [12]. Hence, if we consider only $m_1, \ldots, m_5$, then $mtry = 2$, while the use of all the features from Table 2.1 leads to $mtry = 12$.

A feature selection step is initially carried out on all the features by training an RF, and then selecting the features with the highest importance. The importance of a feature is computed by the sum of the information gain at decision thresholds subject to all the trees [12]. This selection step filters out irrelevant features that would otherwise lead to overfitting.

We can select the top 40-70% of features based on the importance. We used a 10-fold cross validation to verify the fraction of features that seem to give the lowest misclassification error. We tried 40%, 50%, 60%, and 70%, and we found that 40% provides the optimal performance in terms of misclassification error. For feature selection, it is sufficient to use 300-500 trees, because the most relevant features often appear numerous times across all the trees. It also speeds up the selection step. We used 400 trees for feature selection.

3.5 Modifications for Noise Detection

In addition to the six modulation types, the classifiers are also trained to detect noise from signal. It is important to detect noise so that signals identified as noise are not processed at the receiving device. Processing a signal that is noise is a waste of resource for the receiver. Referring to Equation 2.1 of Section 2.1, the additional noise signal is computed using $r[k] = n[k]$. The training data described in Section 3.1 should also include the noise signal data under the column header 'Modulation'. In other words, the noise signal is included as a seventh class variable for the classifiers.

To predict the additional class, we include a feature representing the energy of the signal denoted by en to the training data set. The noise variance, σ_n^2 is defined earlier in Section 2.1.

$$\begin{aligned} e &= \frac{1}{N}\sum_{i=1}^{N} |x[i]|^2 \\ en &= \frac{e}{\sigma_n^2} \end{aligned} \tag{3.6}$$

The training data set is similar to the data set shown in Table 3.1, except there is one more class class variable and one more feature. The new training data set is shown in Table 3.3.

Table 3.3: Example of training data with noise class. The modulation corresponds to the class variable, and the columns to the right of modulation from m_1 to en correspond to the feature variables.

Modulation	$\boldsymbol{m_1}$	$\boldsymbol{m_2}$	$\boldsymbol{m_3}$	**...**	$R[k]$	en
OOK	190	0.05	0.3	...	2.5	34.9
OOK	186	0.12	0.21	...	1.8	32.3
OOK	172	0.08	0.25	...	3.1	29.6
..	..	..	..	..	..	..
BFSK-R2	15.3	0.64	0.03	...	5.4	13.5
BFSK-R2	14.4	0.54	0.08	...	3.3	15.2
BFSK-R2	89.7	0.35	0.12	...	2.48	16.1
..	..	..	..	..	..	..
Noise	56.2	1.3	0.8	...	3.5	34.5
Noise	40.1	1.2	1.1	...	3.2	32.7
Noise	38.5	0.8	0.9	...	1.8	33.3

For FBT, we use en to add a new split in the tree. From Figure 3.13, we can see that values of en for the noise signal is consistently lower than the six modulations. This indicates that en is a useful feature at recognizing noise from the modulations. We performed a worstcase analysis based on en. For example, if en is less than some threshold, then we classify the signal as noise. If the signal is greater than some threshold, then we classify the signal as one of the six modulations. After this initial classification, the tree is constructed the same as before as in Figure 3.3.

From the worstcase analysis plot of Figure 3.14, we observe that at SNR of approximately -8 dB, the maximum value of en intersects with the minimum value of OOK. The threshold value of en is calculated to be 1.0257. Figure 3.15 shows the structure of the tree when the noise signal is included.

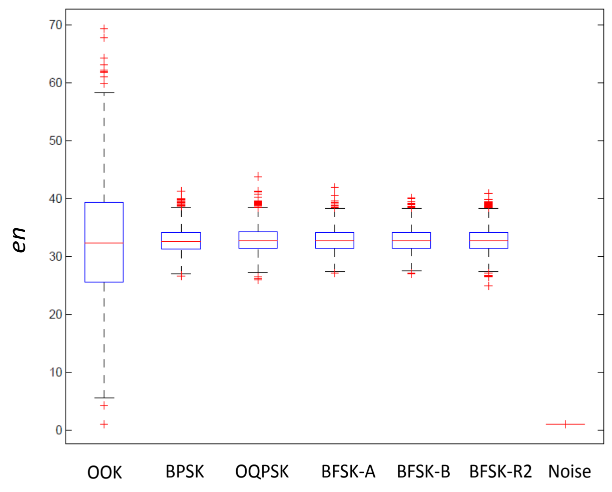

Figure 3.13: Boxplot visualization of *en* for each modulation.

For the CT and RF classifiers, we simply input the new training data set as in Table 3.3 into the same algorithms we described in Sections 3.3 and 3.4.

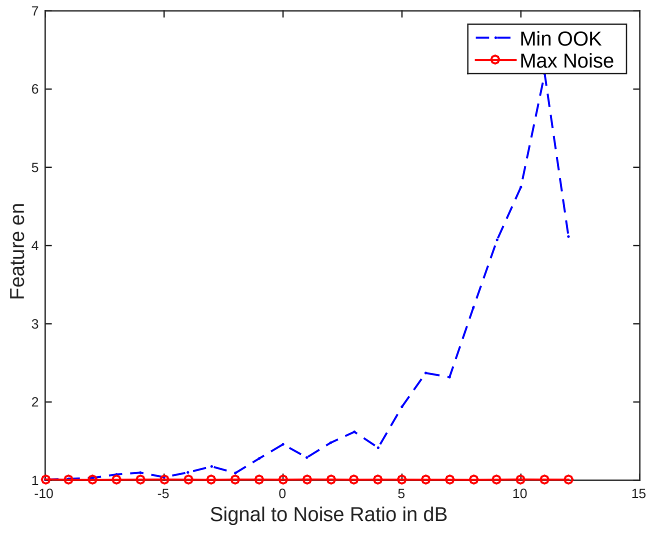

Figure 3.14: Worstcase plot of *en* where minimum value of OOK is compared to maximum value of the noise signal for each SNR.

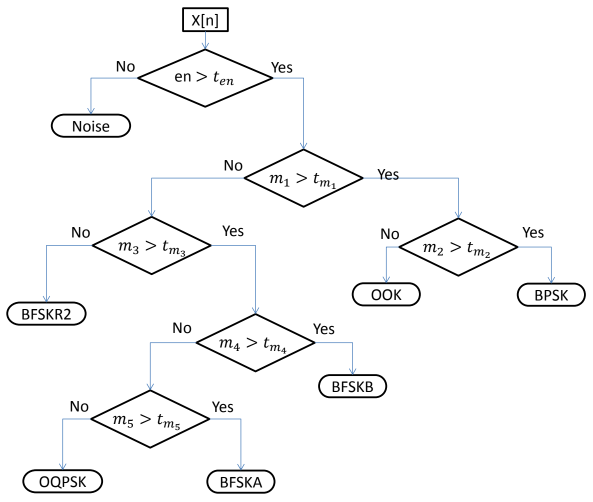

Figure 3.15: Tree structure of FBT with noise signal included.

Chapter 4

Analysis and Results

In this section, we compare the predictive performance of the FBT, CT, and RF classifiers using different sets of features. We also show the difference in performance when including the noise signal as an additional class. To this end, we measure the success rate (SR) of each classifier by applying it on a new data set that was not used for training, and then recording the proportion of correct predictions obtained by the different classifiers.

We generate a training data set based on $P = 50$ values for each feature per modulation between SNR from -25 dB to 13 dB in steps of 1 dB. The testing data set is generated similarly to training, except $P = 200$ is used.

4.1 Analysis on Features From [2]

In the first experiment, we only use the features from [2] and six modulation types. Figure 4.1 shows the SR of each classifier. We observe notable gains for both RF and CT over FBT for SNRs ranging from about -15 dB to 1 dB. RF shows the overall best performance with improvements in SR over FBT of, for example, 32% and 13% (where all improvements are expressed in absolute value) at -5 dB and 0 dB, respectively. Likewise, CT obtained improvements of 20% and 8% at -5 dB and 0 dB, respectively. All three classifiers obtain a SR of approximately one for SNR > 3 dB.

In the second experiment, we use the same features as the first experiment, but the noise signal is included as a seventh class for prediction. As shown in Figure 4.2, the results are similar to the first experiment involving six classes. The RF classifier outperforms the other two classifiers from SNR of -15 dB to 3 dB, and CT outperforms the FBT for the same range of SNR.

Although the structure of the CT is quite different from the FBT as shown in Figures 3.2 and 3.12, if we fit the CT with only high SNR data of > 1 dB, then the structure is almost equivalent to the FBT. The CT fit with SNR > 1 dB and FBT are shown side-by-side in Figure 4.3. The structure of the tree at depth two is identical with only minor differences. The nodes highlighted in orange emphasize that m_5 is chosen before m_4 for the CT. Based on the left subtree after splitting by m_3, small values of m_5 predict

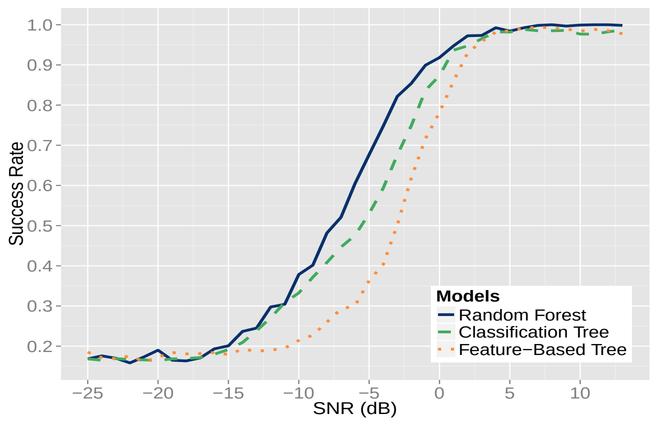

Figure 4.1: Success rates of models based on features from [2] as a function of SNR generated in ggplot2 [17].

OQPSK for both trees. Similarly, small values of m_4 predict BFSK-A and large values of m_5 predict BFSK-B for both trees. From this analysis, it appears that the FBT classifier is similar to the CT if the training data set includes only high SNR signal data.

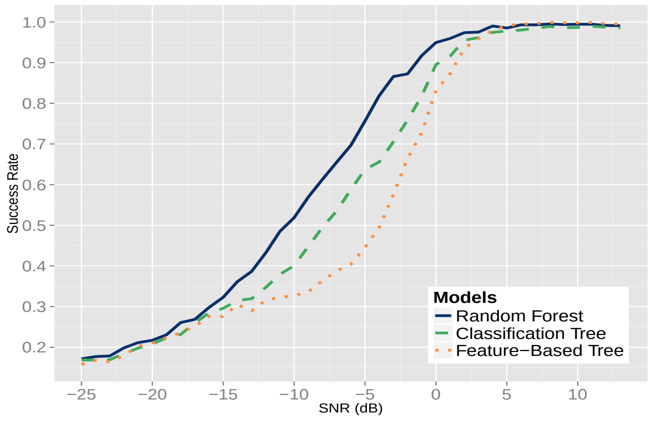

Figure 4.2: SRs based on the features from [2] and prediction for seven classes.

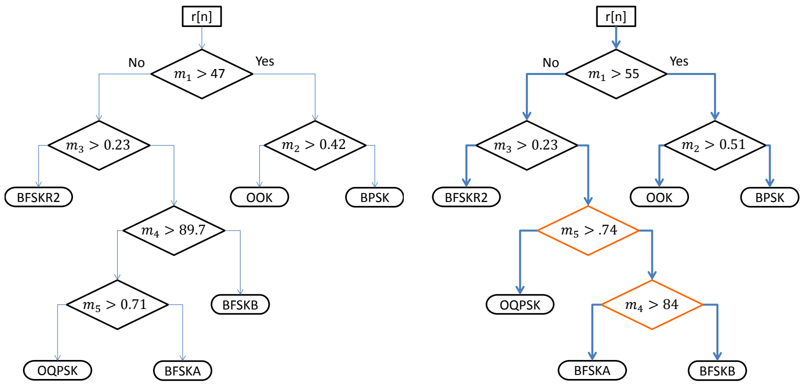

Figure 4.3: The left flow chart represents the FBT with computed threshold values. The right chart corresponds to the CT fit at a high SNR. The main difference is m_5 is used before m_4 with the distinction highlighted in orange.

4.2 Analysis on All Features

In the third experiment, we apply RF and CT based on all the features described in Section 2.2 and summarized in Table 2.1 for six modulations. The corresponding SRs are shown in Figure 4.4. RF obtained a SR of approximately one for SNR > -2 dB. Comparing the SR curves for RF and CT from Figures 4.1 and 4.4, we note the significant additional gain due to the inclusion of the proposed features. The RF and CT classifiers outperform the FBT classifier by a large margin based on a wide SNR range from about -25 dB to 3 dB. Furthermore, the RF classifier achieves best SRs with the gap to CT widened compared to Figure 4.1.

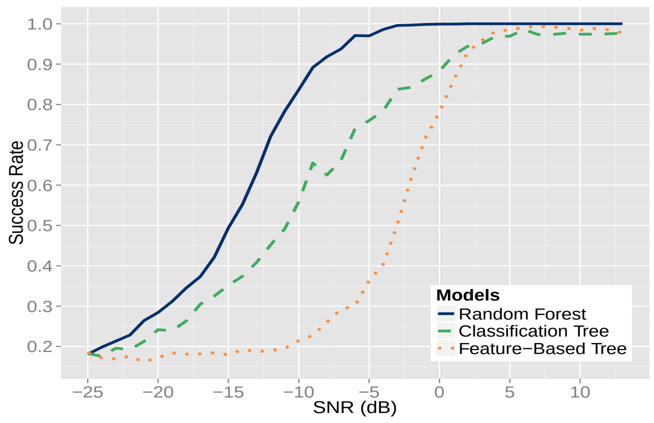

Figure 4.4: Success rates of each model proportional to SNR using all features.

Similar to the third experiment, the fourth experiment includes the noise signal as the seventh class to the data, and we found the results to be very similar. The predictive performance for each classifier is shown in Figure 4.5.

The variable importance plot based on computing the importance of each feature as in Sections 3.4 and [12] is presented in Figure 4.6. The features are ordered by variable importance. From the figure, features with labels beginning with Rk correspond to the magnitude spectrum $|R[k]|$. In fact, $|R[k]|$ at $k = 83, 84, 85 \text{and}, 136$ are within the top 7 features selected. This makes sense since BFSK-B is modulated at a higher intermediate frequency than the remaining modulations. The magnitude spectrum of each modulation type is displayed in Figure 2.3. The figure shows several peaks occurring at discrete-time index k of 83, 84, 85, and 136. Finally, from the variable

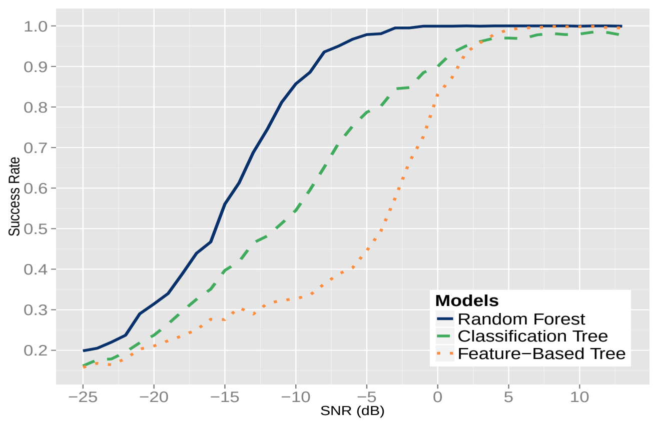

Figure 4.5: SRs based on the all features and prediction for seven classes.

importance figure, we notice that transformation based features γ_{max} and γ_2 also have high importance. Similarly, all features from [2] have high importance.

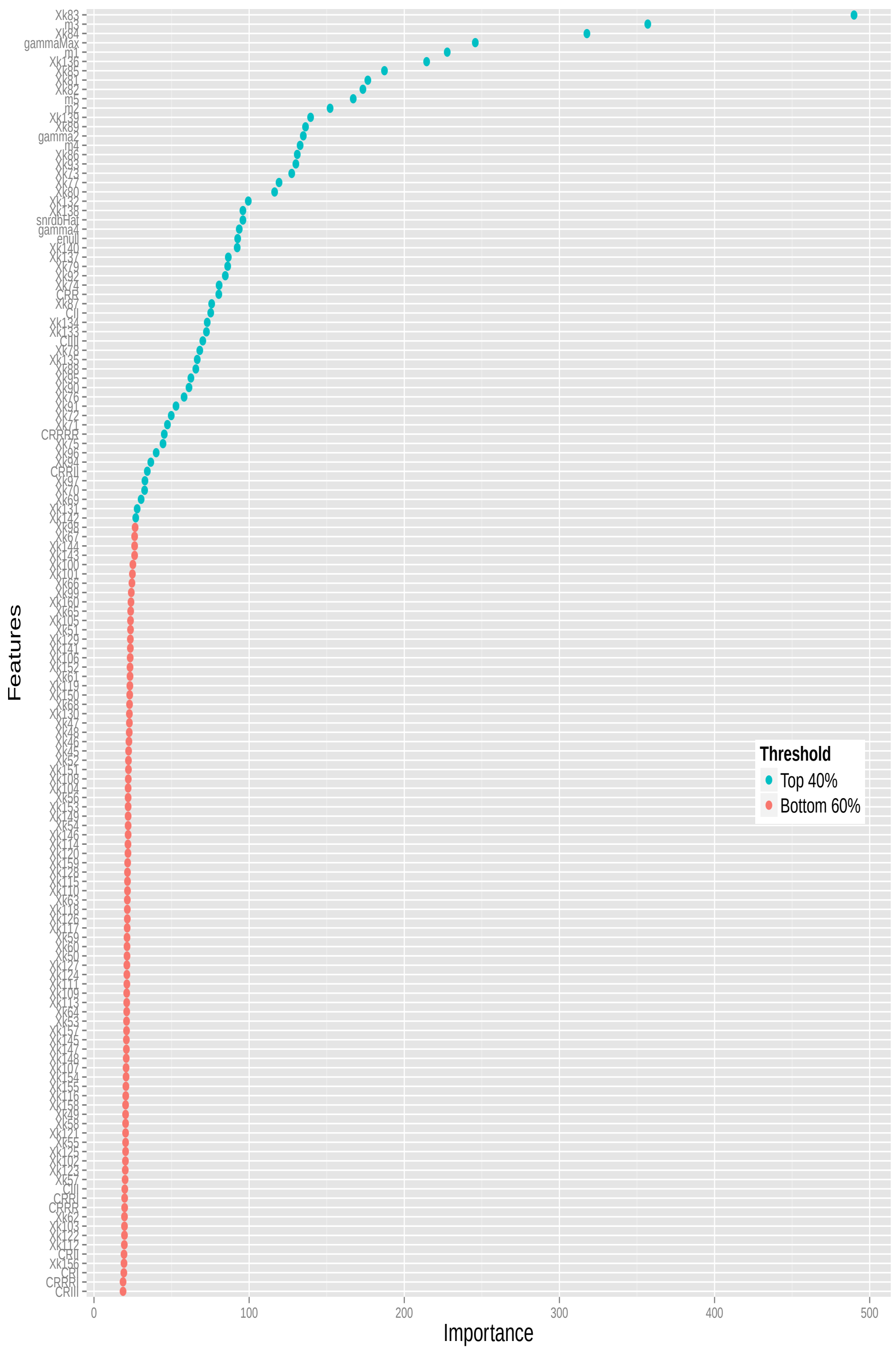

Figure 4.6: Variable importance based on the RF using all the features.

4.3 Further Discussion

Note that the CT classifier does not reach an SR of one even for very high SNRs. One possible explanation is that its thresholds have been influenced by highly noisy training data with low SNR. This observation is supported by the notable improvements that CT achieves over FBT at low SNRs ($\lesssim -2$ dB). Finally, note that, as expected, all classifiers perform almost perfectly well for large SNR levels (SNR $\gtrsim 3$ dB). Hence, the advantage of our proposal is most evident for the more challenging situations of moderate to low SNRs.

The price to be paid for this performance gain is an increase in computation time and storage requirement. The computational complexity of CT and RF classifiers largely depends on the structure of the data, much like many sorting algorithms depend on the initial distribution of the data. That being said, it is still worthwhile to describe the complexity in general. The computational complexity of training a basic implementation of a CT classifier for T training samples and M features is $O(MT\log(T))$ as described on page 199 of [18]. In fact the most basic brute-force approach is $O(MT^2\log(T))$, but is easier to explain first, and then we will explain how the implementation can be improved to be $O(MT\log(T))$.

For each feature variable m, we must compute the entropy using each observation which in total has T observations. Since the observations are not ordered, we must check each remaining $T-1$ observations. Therefore, it takes $T(T-1)$ operations to compute the minimum entropy possible for feature m. Therefore, one split takes roughly MT^2 operations. If we assume that the tree is bushy (in other words it doesn't degenerate to a few long branches) as in the average case of CT, then the depth of the tree is roughly $log(T)$. Thus, in total the number of operations to construct the CT is $MT^2log(T)$ in this brute-force approach. However, if we sort each feature by its observations prior to constructing the tree we can achieve $O(MTlog(T))$.

The average sorting of the observations of one feature is $O(Tlog(T))$ (as is obvious using a standard approach such as quicksort or mergesort). In determining the optimal split, for each feature m, we only need to scan through the observations once in order to find the minimum entropy since the observations are already sorted and we do not need to compare with the remaining operations. So, each split takes roughly MT operations, and assuming a bushy tree the process of constructing the tree is $O(MTlog(T))$ on average.

The computational cost of training a RF classifier is intuitively $O(n_{tree}MT\log(T))$

since the algorithm involves constructing n_{tree} CTs. Training a FBT classifier only costs $O(T\log(T))$, because the features are selected prior to threshold determination (and sorting a single feature variable takes $O(T\log(T))$ on average). Therefore, the CT and RF classifiers require $O(M)$ and $O(n_{tree}M)$ times more operations to train than a FBT, respectively.

The computational cost of a single prediction for the FBT is approximately $O(\log(M))$ evaluations (where $\log(M)$ corresponds to a binary search). The CT classifier with pruning requires $O(\log(M))$ and without pruning requires $O(\log(N)\log(M))$ operations. Therefore, a prediction for RF requires $O(n_{tree}\log(N)\log(M))$ operations.

Since the number of thresholds is fixed for the FBT, the storage cost is $O(1)$. Likewise, the CT with pruning often results in a near constant depth tree regardless of the size of the data set. So, the storage cost of CT with pruning is $O(1)$, and therefore the additional storage requirement of CT is relatively modest. However, the RF requires $O(n_{tree}\log(N))$ in storage requirement as the trees are not pruned. In order to facilitate the implementation of RF, considerable memory allocation may be required.

Chapter 5

Conclusion

In this paper, the classification tree and random forest classifiers are introduced for modulation recognition in the 868 MHz band. The classification tree allows features to appear more than once in the tree leading to an improvement in prediction performance over the feature-based binary tree. The random forest classifier leverages the predictions from a set of classification trees which further improved performance over a single classification tree. Moreover, an additional set of features commonly used in modulation recognition is experimented on and found to improve upon the proposed methods. Based on our findings, both classification tree and random forest attained higher success rates in modulation prediction relative to the feature-based binary tree method when the signal is corrupted with white noise.

Future studies include the addition of more training data for the classifiers, along with an analysis on success rate as a function of the number of observations trained on. This analysis could lead to the implementation of more scalable methods. For example, we plan to implement a map-reduce version of random forest. It would allow data from a distributed file system to be streamed into memory where individual classification trees are fitted and stored in temporary disk until the algorithm is complete.

Bibliography

[1] J. F. Kurose, *Computer networking: a top-down approach featuring the Internet.* Pearson Education India, 2005.

[2] M. Kuba, K. Ronge, and R. Weigel, "Development and implementation of a feature-based automatic classification algorithm for communication standards in the 868 mhz band," in *Global Communications Conference (GLOBECOM), 2012 IEEE*, pp. 3104–3109, IEEE, 2012.

[3] O. A. Dobre, A. Abdi, Y. Bar-Ness, and W. Su, "Survey of automatic modulation classification techniques: classical approaches and new trends," *Communications, IET*, vol. 1, no. 2, pp. 137–156, 2007.

[4] A. Hazza, M. Shoaib, S. Alshebeili, and A. Fahad, "An overview of feature-based methods for digital modulation classification," in *Communications, Signal Processing, and their Applications (ICCSPA), 2013 1st International Conference on*, pp. 1–6, IEEE, 2013.

[5] A. K. Nandi and E. E. Azzouz, "Algorithms for automatic modulation recognition of communication signals," *Communications, IEEE Transactions on*, vol. 46, no. 4, pp. 431–436, 1998.

[6] P. Orponen, "Computational complexity of neural networks: a survey," *Nordic Journal of Computing*, vol. 1, no. 1, pp. 94–110, 1994.

[7] I. The Mathworks, *MATLAB and Communications System Toolbox Release 2014b.* Natick, Massachusetts, United States, 2014.

[8] M. U. Guide, "The mathworks," *Inc., Natick, MA*, vol. 5, p. 333, 1998.

[9] M. D. Wong and A. K. Nandi, "Automatic digital modulation recognition using artificial neural network and genetic algorithm," *Signal Processing*, vol. 84, no. 2, pp. 351–365, 2004.

[10] Z. Wu, X. Wang, Z. Gao, and G. Ren, "Automatic digital modulation recognition based on support vector machines," in *Neural Networks*

and Brain, 2005. ICNN&B'05. International Conference on, vol. 2, pp. 1025–1028, IEEE, 2005.

[11] F. Xie, C. Li, and G. Wan, "An efficient and simple method of mpsk modulation classification," in *2008 4th International Conference on Wireless Communications, Networking and Mobile Computing*, pp. 1–3, 2008.

[12] T. Hastie, R. Tibshirani, and J. Friedman, *The elements of statistical learning*, vol. 2. Springer, 2009.

[13] R. Kohavi *et al.*, "A study of cross-validation and bootstrap for accuracy estimation and model selection," in *Ijcai*, vol. 14, pp. 1137–1145, 1995.

[14] T. M. Therneau, B. Atkinson, and B. Ripley, "rpart: Recursive partitioning," *R package version*, vol. 3, no. 3.8, 2010.

[15] A. Liaw and M. Wiener, "Classification and regression by randomforest," *R news*, vol. 2, no. 3, pp. 18–22, 2002.

[16] L. Breiman, "Random forests," *Machine Learning*, vol. 45, no. 1, pp. 5–32, 2001.

[17] H. Wickham, *ggplot2: elegant graphics for data analysis.* Springer New York, 2009.

[18] I. H. Witten and E. Frank, *Data Mining: Practical machine learning tools and techniques.* Morgan Kaufmann, 2005.